Scientific Research Publishing

Journal of Power and Energy Engineering, 2023, 11, 1-23
https://www.scirp.org/journal/jpee
ISSN Online: 2327-5901
ISSN Print: 2327-588X

Packed Bed Thermocline Thermal Energy Storage for Medium-Temperature Concentrating Solar Systems: Numerical and Experimental Study

Nikolaos Stathopoulos, Nikolaos Papadimitriou, Vassilis Belessiotis, Elias Papanicolaou

Solar and Other Energy Systems Laboratory, Demokritos National Center for Scientific Research, Attiki, Athens, Greece
Email: nistatho@gmail.com, elpapa@ipta.demokritos.gr

How to cite this paper: Stathopoulos, N., Papadimitriou, N., Belessiotis, V. and Papanicolaou, E. (2023) Packed Bed Thermocline Thermal Energy Storage for Medium-Temperature Concentrating Solar Systems: Numerical and Experimental Study. *Journal of Power and Energy Engineering*, **11**, 1-23.
https://doi.org/10.4236/jpee.2023.115001

Received: April 8, 2023
Accepted: April 14, 2023
Published: May 31, 2023

Abstract

Thermal Energy Storage is becoming a necessary component of sustainable energy production systems as it helps alleviate intrinsic limitations of Renewable Energy Sources, such as intermittent use and mismatch between power demand and supply. This paper discusses a packed bed thermocline tank as a thermal energy storage solution. Firstly, this paper presents the development of a numerical model calculating heat transfers within the tank, based on a discretization over several nodes and the nodal formulation of the heat balance equation. The model considers a filler material and a heat transferring fluid and uses the finite difference method to calculate the temperature evolution of the two media across the tank. The model was validated with two different packed bed systems from the literature during a discharging process, presenting a good fit with the experimental results. Secondly, the experimental packed bed is presented and characterized for a charging cycle from ambient temperature to approximately 180˚C. The charging experiment was accurately reproduced with the numerical model requiring minimal computational time. Two additional charging modes were simulated with different inlet HTF conditions: constant temperature and varying temperature following the profile produced by a thermal solar collector field. The temperature profiles obtained from the three charging modes were analysed and compared to each other. The proposed numerical and experimental tools will be used in future studies for a better understanding of the design and operating conditions of packed bed thermal energy storage systems.

Keywords

Thermal Energy Storage, Packed Bed, Numerical, Model, Experimental

1. Introduction

Systems exploiting Renewable Energy Sources (RES), such as solar, are strongly affected by intermittent meteorological conditions, therefore presenting varying energy availability and imbalance between energy demand and supply. Thermal Energy Storage (TES) applications can help alleviate this issue by storing energy in periods with lower demand and/or higher supply and releasing it during peak demand periods [1] [2]. In addition, TES technology can result in CO_2 and cost reduction by making sure energy is used when it is less expensive and when renewable energy presents an increased share in the mix. Furthermore, TES contributes to the increase of the efficiency, reliability, and security of energy systems.

Currently, application of TES technology can be found in the building sector (HVAC, DHW), the industrial sector (chemical industry, food industry, etc.) and power production (solar thermal power plants) [2]. Recent advances in the field propose pumped thermal electricity storage, a technology that uses TES tanks (usually large scale packed-bed reservoirs) to store electricity produced heat and later convert it back to electricity [3] [4].

Focusing on thermal solar energy systems, there are three main forms of TES applications: sensible, latent and thermochemical storage. TES in sensible form presents several attractive advantages: simpler and less expensive implementation, completely reversible charging and discharging operation and limited degradation over a repeated number of thermal cycles [5] [6].

The most mature technologies today are those based on the first option, *i.e.*, sensible form, with the most widespread application being the Domestic Hot Water (DHW) tanks (solar water heaters), using water as the storage medium. However, at temperatures above 100˚C, usually coupled with concentrating solar systems for industrial and power generation applications, the use of water is no longer cost-effective, making the use of other materials necessary [7]. The design of a sensible TES system is an elaborate process that includes several considerations, such as the required application field (usually defining the temperature span), technical aspects (available volume, storage capacity, compatibility between selected materials etc.) and economic factors (cost of material and tank assembly, availability of material, etc.) [8].

Among available types of sensible TES systems, several studies report the benefits of packed bed applications, including high reliability and operability [9], being simpler to develop [10] and exhibiting improved performance compared to other options, due to a high surface area for heat transfer [11]. The packed bed configuration consists of a single tank solution, containing a fixed bed of filler solid material, used as the Filler Material (FM), and a second medium traversing the container, acting as the Heat Transferring Fluid (HTF) [12] [13] [14] [15]. The HTF is therefore used for the charging and the discharging process of the packed bed, as heat transfer occurs through direct surface contact of the FM and the HTF [16]. The use of the FM reduces the amount of needed fluid in the

tank, thus reducing the cost and the volume of the TES application. Furthermore, the heat exchange between the filler material and the HTF creates temperature stratification, *i.e.*, thermocline, in this way removing the need for a second storage tank.

The design of an appropriate packed bed TES system, as well as the choice of the FM and HTF materials, is a challenging task as undesired effects are to be avoided, such as insufficient storage capacity, overheating of the system, overpressure, etc. [8]. Within the Solar and Other Energy Systems Laboratory at the National Center for Scientific Research "Demokritos", a research and innovation infrastructure has been developed for the production and storage of medium-temperature thermal energy. Among other elements, the infrastructure includes a solar thermal parabolic collector and a packed bed TES system. The exploitation of this infrastructure, including the investigation of its performance and effective control strategies scenarios for specific building and industrial applications, requires the development of advanced numerical tools that simulate the heat transfer phenomena in an accurate and timely manner.

Within this context, the present study describes the numerical method used to develop a model that reproduces the performance of a packed bed TES system. The model is validated with the use of experimental data from two different literature studies. Afterward, the research and innovation infrastructure is introduced, focusing on the packed bed tank. At present, few studies examine the performance and the potential of solar thermal applications using magnetite ore as the filler material of a coupled TES system. A thermal charging cycle of this type of system is presented, offering novel experimental data. The characteristics of the tank are introduced to the developed model and the same charging cycle is numerically reproduced. Three different charging modes are investigated, providing different charging profiles, by altering the inlet HTF temperature (constant and varying). Results obtained from the experimental charging and the additional simulated scenarios are examined and compared, whereas useful thermal performance parameters are calculated.

2. Numerical Model

2.1. Description

A numerical model was developed in this study with the aim to simulate the performance of a TES tank. The model considers cylindrical geometry for the tank and spherical geometry for the filler material. It is based on the formulation of the heat balance equations for the filler and transfer media that are solved under MATLAB-Simulink environment [17] [18] [19]. Solution of the model lies on the discretisation of the investigated medium into a specific number of layers (nodes) and the subsequent application of the energy balance equation on each of them.

The tank is represented as a vertically placed cylinder, fully packed with the filler material, while the HTF flows around it and through the void fraction (**Figure 1**).

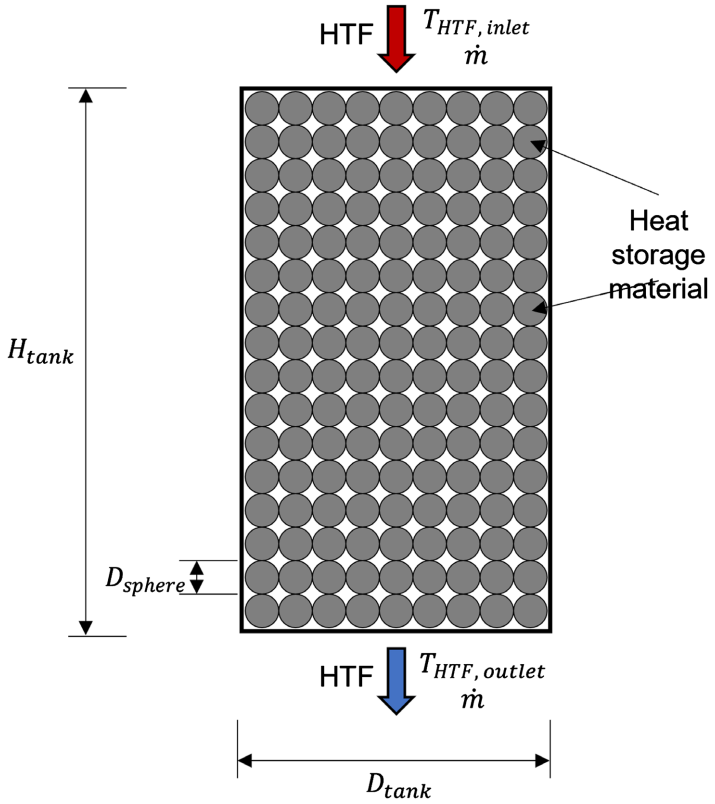

Figure 1. Schematic representation of the thermal energy storage tank.

The HTF flow inside the tank is considered uniform and in one dimension (across the axial direction). The FM is considered as a perfect sphere with temperature uniformity across it. The TES tank is considered as a porous medium with a uniformly distributed FM, having a porosity φ. The number of nodes, n, is taken equal to the round quotient of the height of the tank by the diameter of the filler sphere. Volume expansion and shrinkage during the charging and discharging phase respectively are neglected. Lastly, radiation related heat transfer is also neglected.

The energy balance equations are expressed for the HTF and the FM, taking into account applicable heat transfer phenomena. Figure 2 illustrates the heat transfer processes for consecutive nodes (*i.e.*, $i-1$, i, $i+1$) occurring between the HTF, the FM and the surrounding.

Based on the aforementioned considerations and assumptions, the energy balance equation for the HTF at the ith node is expressed as follows:

$$\begin{aligned}&\rho_a c_{p,a} V_a \frac{\mathrm{d}T_a}{\mathrm{d}t}\\&= \varphi \dot{m} c_{p,a}\left(T_{a,i-1}-T_{a,i}\right)+\frac{\varphi k_a A_{i+1,i}}{\Delta y_{i+1,i}}\left(T_{a,i+1}-T_{a,i}\right)+\frac{\varphi k_a A_{i-1,i}}{\Delta y_{i-1,i}}\left(T_{a,i-1}-T_{a,i}\right)\\&\quad -UA_{s,i}\left(T_{a,i}-T_{amb}\right)+h_{sf}A_{sf}\left(T_{p,i}-T_{a,i}\right)\end{aligned} \tag{1}$$

Similarly, the energy balance equation for the FM at the ith node is expressed as follows:

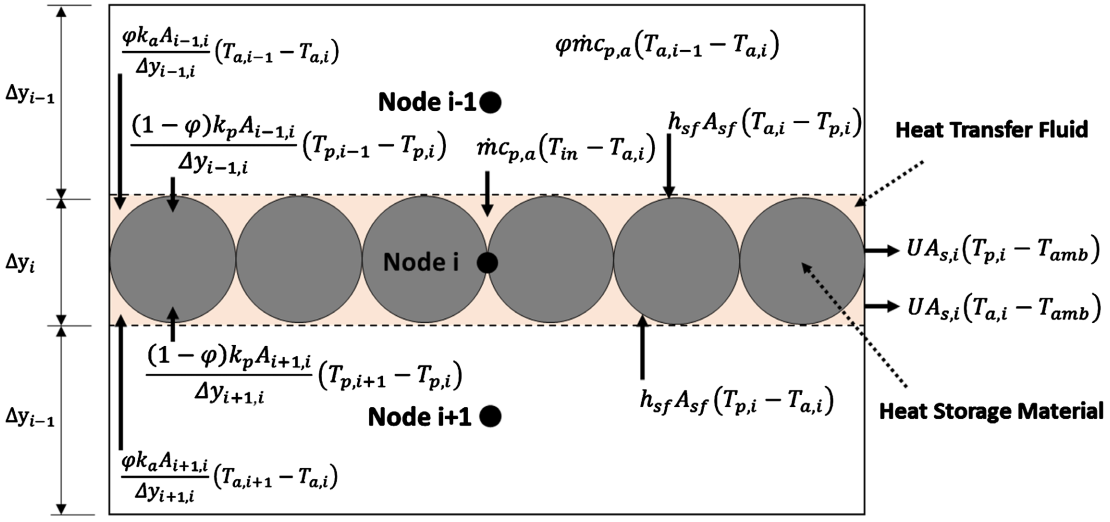

Figure 2. Nodal discretisation of the TES tank and representation of heat transfer phenomena.

$$\begin{aligned}&\rho_p c_{p,p} V_p \frac{\mathrm{d}T_p}{\mathrm{d}t}\\&=\frac{(1-\varphi)k_p A_{i+1,i}}{\Delta y_{i+1,i}}\left(T_{p,i+1}-T_{p,i}\right)+\frac{(1-\varphi)k_p A_{i-1,i}}{\Delta y_{i-1,i}}\left(T_{p,i-1}-T_{p,i}\right)\\&-UA_{s,i}\left(T_{p,i}-T_{amb}\right)+h_{sf}A_{sf}\left(T_{a,i}-T_{p,i}\right)\end{aligned} \tag{2}$$

where T is the node temperature, ρ is the density, k is the thermal conductivity, C_p is the specific heat capacity, V is the node volume, A is the node cross area, Δy is the distance between two consecutive nodes, φ is the porosity, U is the natural convective heat transfer coefficient at the vertical surface of the tank, h_{sf} is the interstitial heat transfer coefficient, A_s is the wall surface of the cylinder, A_{sf} is the superficial area per unit volume area and $\dot{m}$ is the fluid flow rate. Subscripts a and p refer to the HTF and FM respectively, while i represents the axial nodal position.

Equations (1) and (2) are then discretised with the use of the implicit finite difference method.

For the HTF at the ith node this is expressed as follows:

$$\begin{aligned}&\rho_a c_{p,a} V_a \frac{T_{a,i}^t - T_{a,i}^{t-dt}}{\Delta t}\\&=\dot{m}c_{p,a}\left(T_{in}^t-T_{a,i}^t\right)+\varphi\dot{m}c_{p,a}\left(T_{a,i-1}^t-T_{a,i}^t\right)+\frac{\varphi k_a A_{i+1,i}}{\Delta y_{i+1,i}}\left(T_{a,i+1}^t-T_{a,i}^t\right)\\&+\frac{\varphi k_a A_{i-1,i}}{\Delta y_{i-1,i}}\left(T_{a,i-1}^t-T_{a,i}^t\right)+UA_{s,i}\left(T_{a,i}^t-T_{amb}^t\right)+h_{sf}A_{sf}\left(T_{p,i}^t-T_{a,i}^t\right)\end{aligned} \tag{3}$$

For the FM at the ith node this is expressed as follows:

$$\begin{aligned}&\rho_p c_{p,p} V_p \frac{T_{p,i}^t - T_{p,i}^{t-dt}}{\Delta t}\\&=\frac{(1-\varphi)k_p A_{i+1,i}}{\Delta y_{i+1,i}}\left(T_{p,i+1}^t-T_{p,i}^t\right)+\frac{(1-\varphi)k_p A_{i-1,i}}{\Delta y_{i-1,i}}\left(T_{p,i-1}^t-T_{p,i}^t\right)\end{aligned}$$

$$+UA_{s,i}\left(T_{p,i}^{t}-T_{amb}^{t}\right)+h_{s}A_{sf}\left(T_{a,i}^{t}-T_{p,i}^{t}\right) \quad (4)$$

U, the natural convective heat transfer coefficient at the vertical surface of the tank, is calculated based on the following equation [13]:

$$U=\frac{Nuk_{air}}{d_{p}} \quad (5)$$

where Nu the Nusselt number is taken from [20]:

$$Nu=0.6Re^{0.5}Pr^{1/3} \quad (6)$$

And Re the Reynolds number and Pr the Prandtl number [21]:

$$Re=\frac{4\dot{m}d_{p}}{\pi D_{t}^{2}\mu} \quad (7)$$

where D_t is the tank diameter, d_p the solid sphere diameter, and μ the fluid viscosity.

In a similar manner, h_{sf}, the interstitial heat transfer coefficient, is calculated using [22] Equation (5), where Nusselt number is taken from [22]:

$$Nu=2+1.8Re^{0.5}Pr^{1/3} \quad (8)$$

A_{sf}, the superficial area per unit volume area, is calculated as [23]:

$$A_{sf}=\frac{6V_{s}\left(1-\varphi\right)}{d_{p}} \quad (9)$$

This formulation leads to a system of linear equations that are scripted in MATLAB environment and solved by matrix algebra techniques. Based on this, the HTF and FM temperatures for each node are calculated at every time step, using as inputs the HTF inlet temperature, the HTF flow rate and the temperatures of the layers at the previous time step. For the first time step, an initial state of the tank is set, for example as fully charged/discharged or with a specific temperature profile.

2.2. Validation

The presented numerical study is validated through a twofold comparison of obtained results with experimental data from the literature. Specifically, the conditions observed during the experiments of Pacheco *et al.* [24] and Hoffmann *et al.* [25] are used in the simulation. This section briefly presents the experimental work from these two studies and compares the experimental and simulated results (temperature evolution at various axial points in the tank over time). **Table 1** lists the characteristics of the developed systems from Pacheco *et al.* [24] and Hoffmann *et al.* [25].

2.2.1. Validation, Pacheco *et al.*

Pacheco *et al.* [24] developed a thermocline experimental system as part of a larger TES application. The tank exterior is made of steel and has a height of 6.1 m and a diameter of 3.0 m. The insulation of the tank consisted of 23 cm of fiberglass on the sides and 20 cm of calcium silicate ridged block at the top of the

Table 1. Characteristics of two different thermocline tanks from literature for model validation.

Parameter	Pacheco *et al.* [24]	Hoffmann *et al.* [25]
Energy	2.3 MWh	8.3 kWh
Filler material	Quartzite and silica filter sand	Quartzite rock
Heat transfer fluid	Molten salt	Rapeseed oil
Tank height	6.1 m	1.8 m
Tank diameter	3.0 m	0.4 m
Porosity	0.22	0.41
Discharge time	2 h	3.5 h
Temperature of HTF, charge	390˚C	210˚C
Temperature of HTF, discharge	290˚C	160˚C

tank. The FM is a mixture of quartzite and silica filter sand (2:1 ratio) and the HTF is molten salt (a nearly eutectic mixture of sodium nitrate and potassium Nitrate). The final void fraction of the tank is 0.22 and the total storage capacity reached 2.3 MWh.

The salt was heated to approximately 390˚C and was then was poured to the tank from the bottom for the charging process; during the discharging process the temperature of the salt was 290˚C. Measurements of the temperature at different axial positions along the tank were taken (middle radial point) every 30 min during the discharging phase, for a total discharge phase of two hours.

The initial state of the tank for the simulation is set based on the experimental values at time 0 h. The comparison is performed for the remaining experimental values during the 2 h discharge process, with a 30 min interval. The inlet temperature of the HTF is considered constant over the course of the experiment and taken equal to 290˚C. Based on these conditions and the tank characteristics, the discharge process is simulated with the use of the numerical model. **Figure 3** illustrates the experimental and numerical results for the temperature distribution of the HTF across the TES tank (axial direction).

It can be noted that the developed numerical model manages to accurately reproduce the experimentally observed temperature evolution at different axial points of the tank, for several time instances during the discharging process. The minor observed differences, for instance for time $t = 2$ h at $H = 4.9$ - 6.1 m, are consistent with findings from the literature ([26] fig. 13, [27] fig. 3) and can be attributed to experimental uncertainties.

2.2.2. Validation, Hoffmann *et al.*

Hoffmann *et al.* [25] developed a laboratory scale thermocline TES tank, 1.8 m high and 0.4 m in diameter. The tank is insulated with a 20 cm aluminum foil covered rock wool layer. The FM is quartzite rock and the HTF is rapeseed oil. The void fraction of the developed apparatus is 0.41 and the total storage capacity

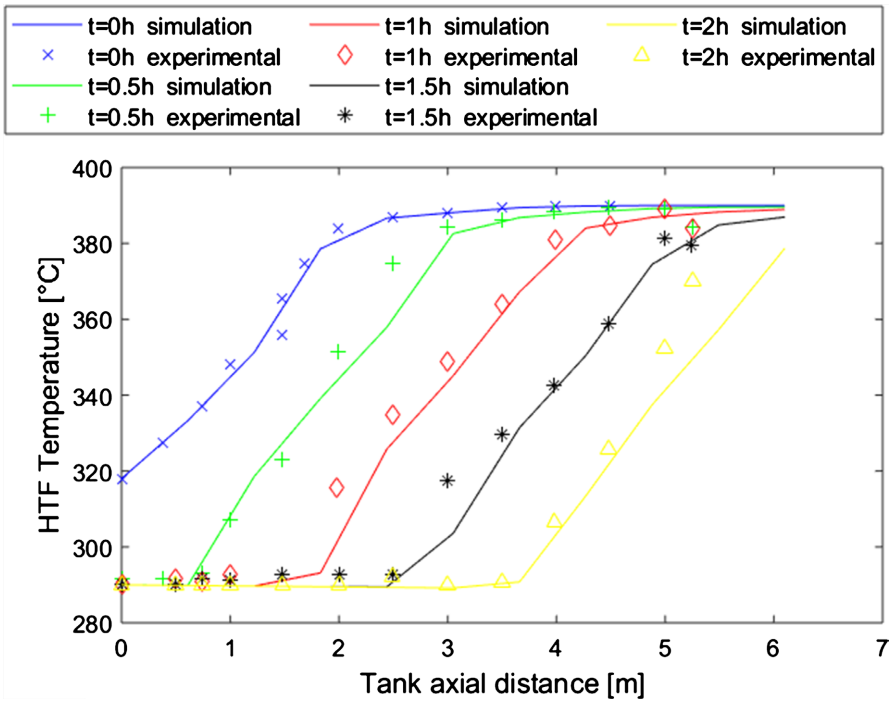

Figure 3. Comparison between numerical and experimental results from Pacheco *et al.* [24], temperature profile during discharging process.

is 8.3 kWh. The instrumentation consisted of 32 thermocouples placed at the axial direction of the tank and several additional sensors along the radial axis, allowing monitoring the temperature evolution across the TES unit over time. The temperature of the heat transfer fluid during the charging and the discharging phases was 210˚C and 160˚C respectively.

Similar to the previous validation study, the initial state of the tank is equal to the experimental measurements at time $t = 0$ h and the remaining experimental data are used to validate the model. A 3.5 h discharge phase is simulated, with a constant inlet HTF temperature of 160˚C. **Figure 4** presents the experimental and numerical results of the HTF temperature evolution at the axial direction of the tank, with a 30 min interval. Results demonstrate anew the good agreement between experimental data and numerical prediction, offering a second validation of the proposed numerical work. Minor discrepancies are observed, for instance for time $t = 1$ h and $t = 1.5$ h, also reported in the results of Hoffmann *et al.* ([25], fig. 8), probably related to experimental uncertainties.

Through this approach, the TES tank numerical model is compared with two experimental systems ([24] [25]), holding different sizes, FM, HTF, as well as discharging periods and inlet HTF temperatures. This consistent study validates the proposed numerical method and its outcomes in a rigid manner.

3. Description of TES Tank

The investigated application concerns a sensible heat packed bed TES (**Figure 5**). Its cylindrical part is divided into three separate chambers carrying the filler

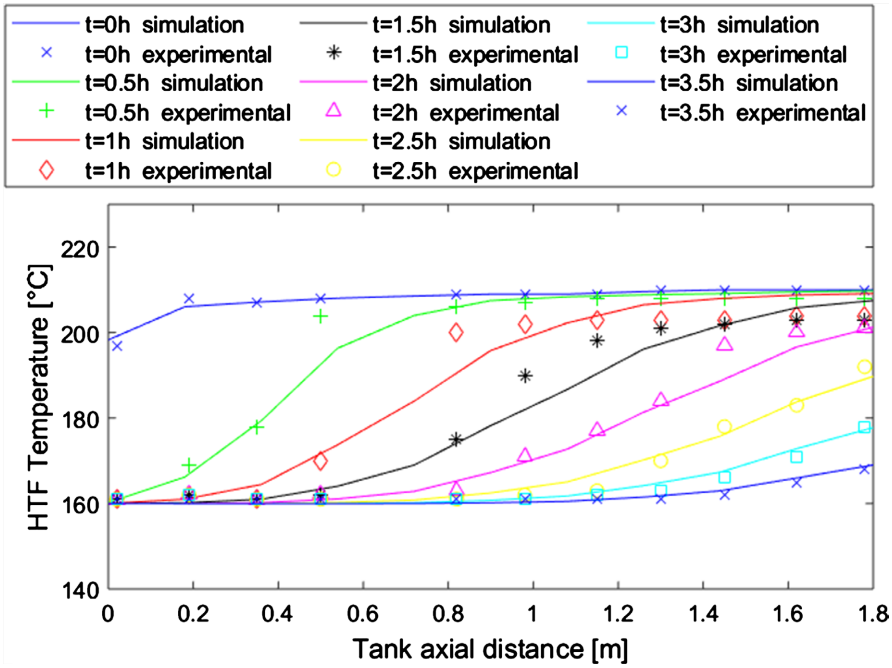

Figure 4. Comparison between numerical and experimental results from Hoffmann *et al.* [25], temperature profile during discharging process.

Figure 5. The experimental 2 m^3 magnetite TES tank (left) and internal structural details and flow configuration during charging (right).

material and is enclosed at the two ends by suitably designed conical parts with internal dividers, in order to achieve a more uniform flow distribution at the inlet and exit. The TES tank contains magnetite ore [28] as the filler material and Therminol® SP [29] as the heat transfer fluid. Magnetite ore (Fe_3O_4) is a common substance in the course of iron extraction. It is abundantly available, inexpensive (0.18 $/kg, [30]), non-flammable, low-permeable and has high density and thermal conductivity values [31]. These characteristics make it an excellent

candidate as a filler material, however only a handful of studies investigate its potential ([31] [32] [33] [34] [35]). It should be noted though that this storage technology is being used in an actual concentrating solar thermal plant, operating on an organic Rankine cycle (ORC), driven by a Fresnel collector solar field [36].

The TES tank has a cylindrical shape (vertically placed), with a height of 2.39 m and an internal diameter of 1.1 m; the porosity φ is 0.39. The tank is thermally insulated with a 13 cm thick rock wool layer. **Table 2** resumes the properties of the FM and HTF.

An elaborate instrumentation study resulted in the positioning of 23 thermocouples across the axial direction of the tank, in the middle radial point, that are used to obtain the temperature profile of the TES system (**Figure 6**). Two additional thermocouples are placed at the inlet and outlet point of the tank to monitor the HTF at the entrance and exit positions of the tank.

4. Results and Discussion

Three different charging scenarios of the TES tank are presented in this section. The first one concerns a charging process with an increasing inlet HTF temperature at a nearly linear rate. This mode was the one experimentally executed, corresponding to electric heating of oil and then reproduced using the validated numerical model. It is representative of an initial charging cycle, whereby the tank (oil and filler material) is initially at ambient temperature.

The second charging mode, which is the one most often encountered in the literature, considers a constant inlet temperature of 180˚C for the HTF from the beginning until the end of the charging process. The heating of the tank with an increased HTF temperature from the start of the process leads to a significantly faster charging, as the HTF at the outlet point of the tank reaches its maximum temperature in less than 1 h.

The third charging mode concerns a varying temperature based on realistic conditions, representative of heating from a solar-collector field. Previous studies have captured this profile for a typical operation day and have found that a

Table 2. Properties of Therminol® SP as HTF and magnetite ore as FM.

	Therminol® SP (at 150˚C)	Magnetite ore
Density (kg/m^3)	784	5186
Specific heat capacity (kJ/(kgK)	2.37	0.85
Thermal conductivity (W/mK)	0.1133	2.825
Liquid viscosity (mPa·s)	1.29	-
Operating Temperature (˚C)	−28 to 290	-
Equivalent diameter of magnetite particles (mm)	-	10
Porosity φ of packed bed	-	0.39

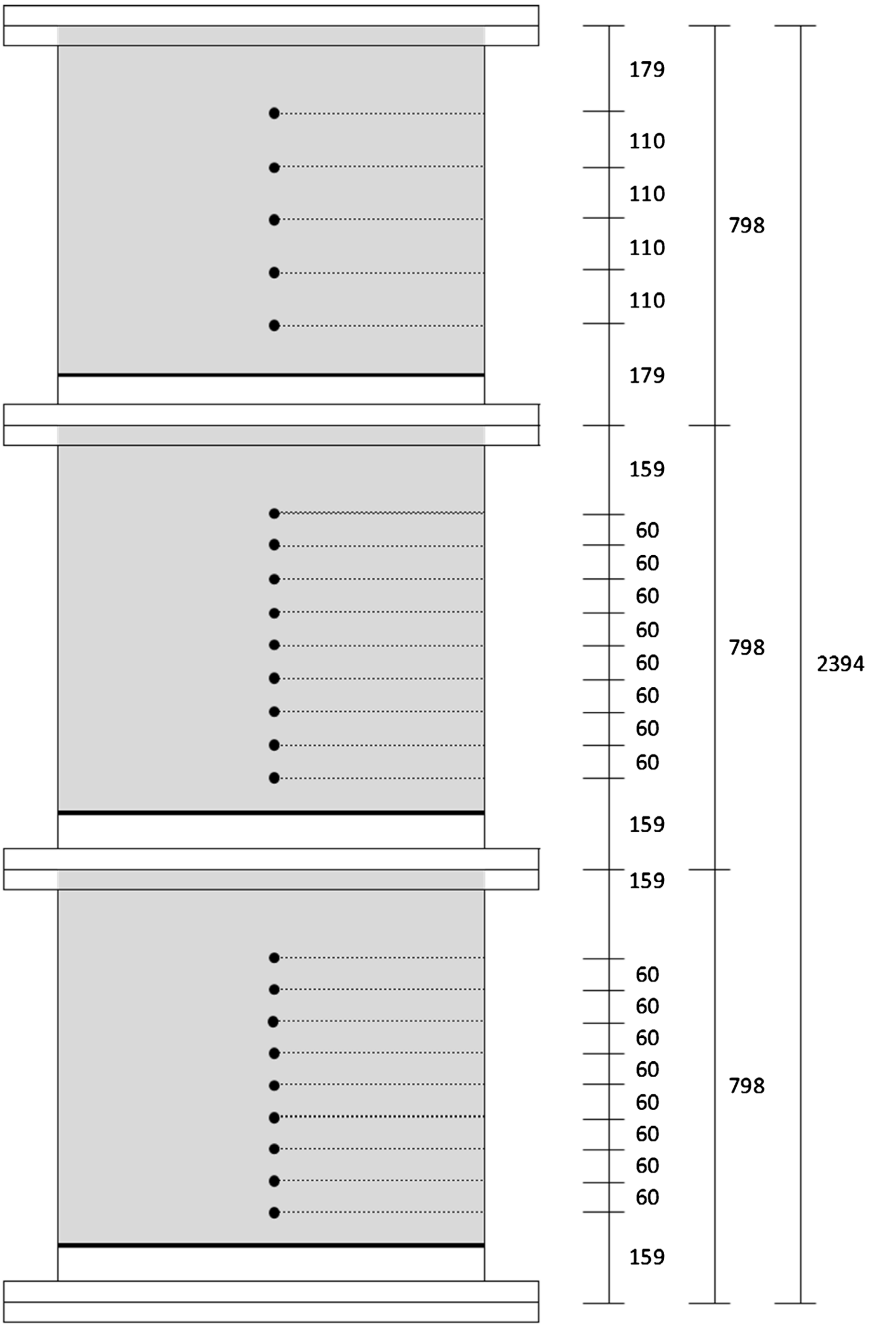

Figure 6. Schematic representation of the position of thermocouples inside the TES tank (all distances are represented in cm).

sixth-degree polynomial adequately approximates it [37]. The polynomial has the following form:

$$T_{in} = a_0 t + a_1 t + a_2 t^2 + a_3 t^3 + a_4 t^4 + a_5 t^5 + a_6 t^6 \quad (10)$$

where t refers to time (in min) and a_0 to a_6 are presented in **Table 3**.

Figure 7 presents the inlet HTF temperature for the different investigated charging modes. The initial temperature of the tank was set to approximately 27˚C and the HTF flow rate was 2.2 kg/s for all three cases. The characteristics of

Table 3. Polynomial coefficients in Equation (10), solar collector field.

Coefficient	Value (solar heating)
a_0	$-1.420431356898 \times 10^{-3}$
a_1	$2.103778934489 \times 10^{-3}$
a_2	$3.051129914167 \times 10^{-5}$
a_3	$-1.593109661544 \times 10^{-7}$
a_4	$2.808978144742 \times 10^{-10}$
a_5	$-1.011443517559 \times 10^{-13}$
a_6	$-1.814326134579 \times 10^{-16}$

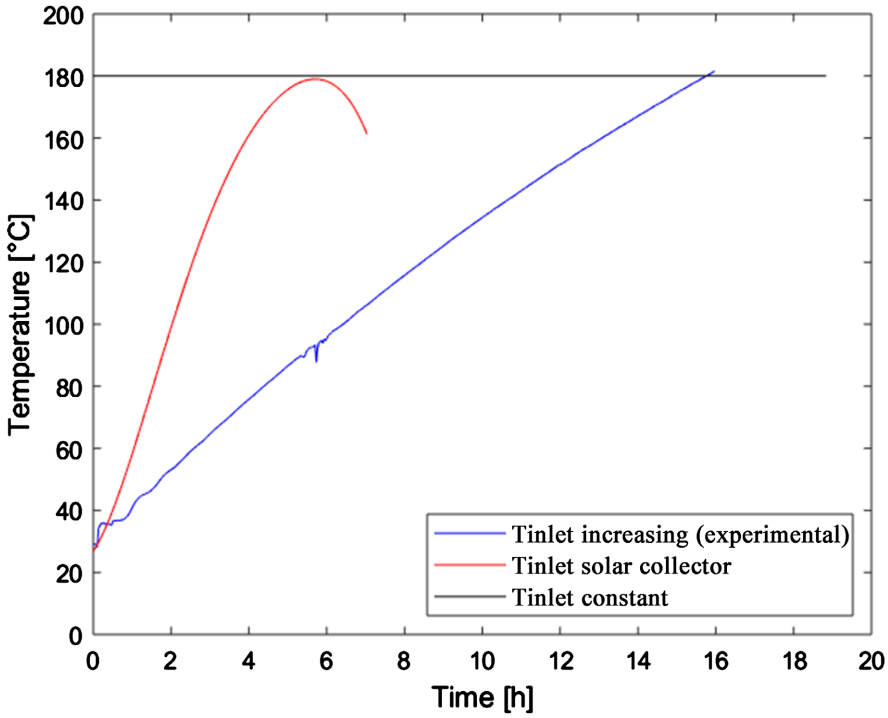

Figure 7. Inlet HTF for the different charging scenarios.

the packed bed TES system, as well as its initial state, HTF inlet temperature and flow rate were introduced to the numerical model and the three charging cycles were simulated until the TES tank reached a fully charged state at an approximate temperature of 180˚C. Regarding the third scenario (solar collector field), the simulation was carried out until t = 6 h, given the fact that the subsequent period, with inlet temperature reducing with time, would result in the gradual discharging of the TES tank.

Figure 8 focuses on the first scenario and compares the experimental and numerical results for the HTF temperature at different axial positions of the tank for selected time intervals (every 4 h). The experimental values represent a charging cycle of a magnetite-based TES system and are a novel addition to the literature. It can be observed that, once again, the numerical model reproduces

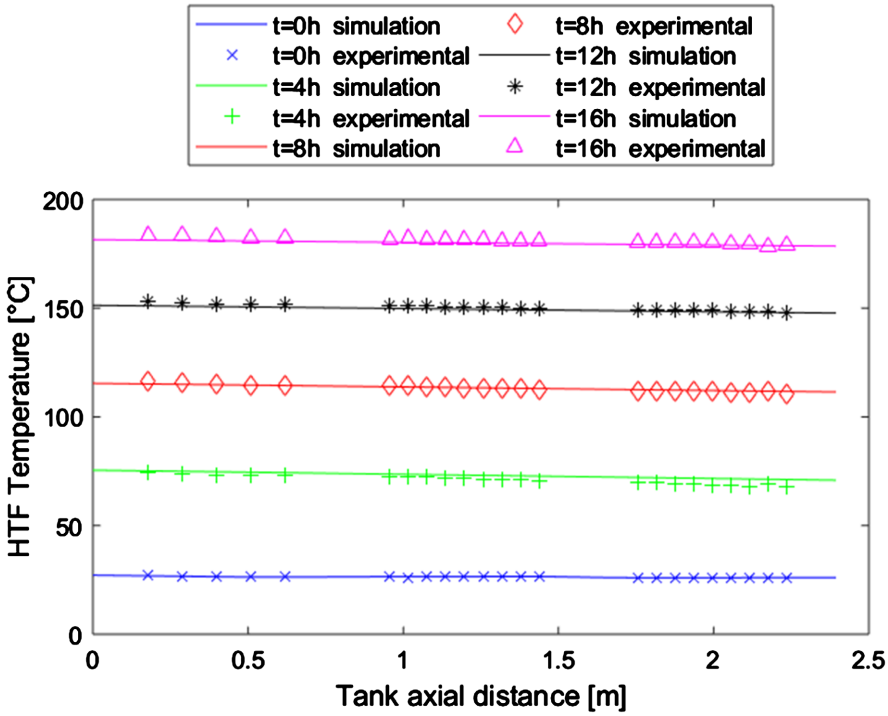

Figure 8. Comparison between numerical and experimental results for packed bed TES, temperature profile during charging process, scenario 1, increasing inlet HTF temperature.

the behaviour of the TES system accurately, in this case during a charging process with a varying inlet HTF temperature.

Thermal performance parameters showing the total amount of energy stored in the tank, the instantaneous charging efficiency and the thermal stratification number are also investigated for the three modes.

The total energy stored is calculated as follows [38]:

$$Q = \sum_{i=1}^{i=n} \dot{m}_{\mathrm{HTF}} c_{p,\mathrm{HTF}} \Delta T \Delta t_i \tag{11}$$

where Q is the energy stored, $\dot{m}_{\mathrm{HTF}}$ and $c_{p,\mathrm{HTF}}$ are the flow rate and specific heat capacity of the HTF, ΔT is the inlet and outlet temperature difference of the HTF, Δt_i is the time interval in the simulations and t_c is the overall charging time, $t_c = n^* \Delta t_i$ with n the number of intervals.

The instantaneous (or transient) charging efficiency η is calculated as follows [38]:

$$\eta = \frac{T_{in} - T_{out}}{T_{in} - T_{ini}} \tag{12}$$

where T_{in}, T_{out} are the inlet and outlet temperatures of the HTF and T_{ini} is the initial temperature of the storage.

Furthermore, whereas according to the study by Lou *et al.* [39], the above parameter belongs to the class of performance indicators reflecting the quantity of the stored thermal energy, there are other factors characterizing the thermal stratification level, such as the stratification number *Str*. This is a time-dependent parameter, defined as [39]:

$$Str(t) = \frac{\overline{(\partial T/\partial z)_t}}{(\partial T/\partial z)_{\max}} \tag{13}$$

where *Str* is the stratification number, $\overline{(\partial T/\partial z)_t}$ the mean temperature gradient for each radial position at each time interval and $\overline{(\partial T/\partial z)_{\max}}$ the maximum temperature gradient during the charging process.

This parameter is used here also to compare the different charging modes.

Table 4 summarises the calculated charging time and total energy stored for the three investigated charging modes. The first mode results in a higher energy storage, followed by the third one, while the second mode presents the lowest value, even though being much faster. However, given the different charging conditions, the tank does not reach a similar state at the end of each process. The stored energy values are therefore presented for the sake of completeness of information but are not directly comparable.

Figure 9 presents the axial temperature distribution for the three charging

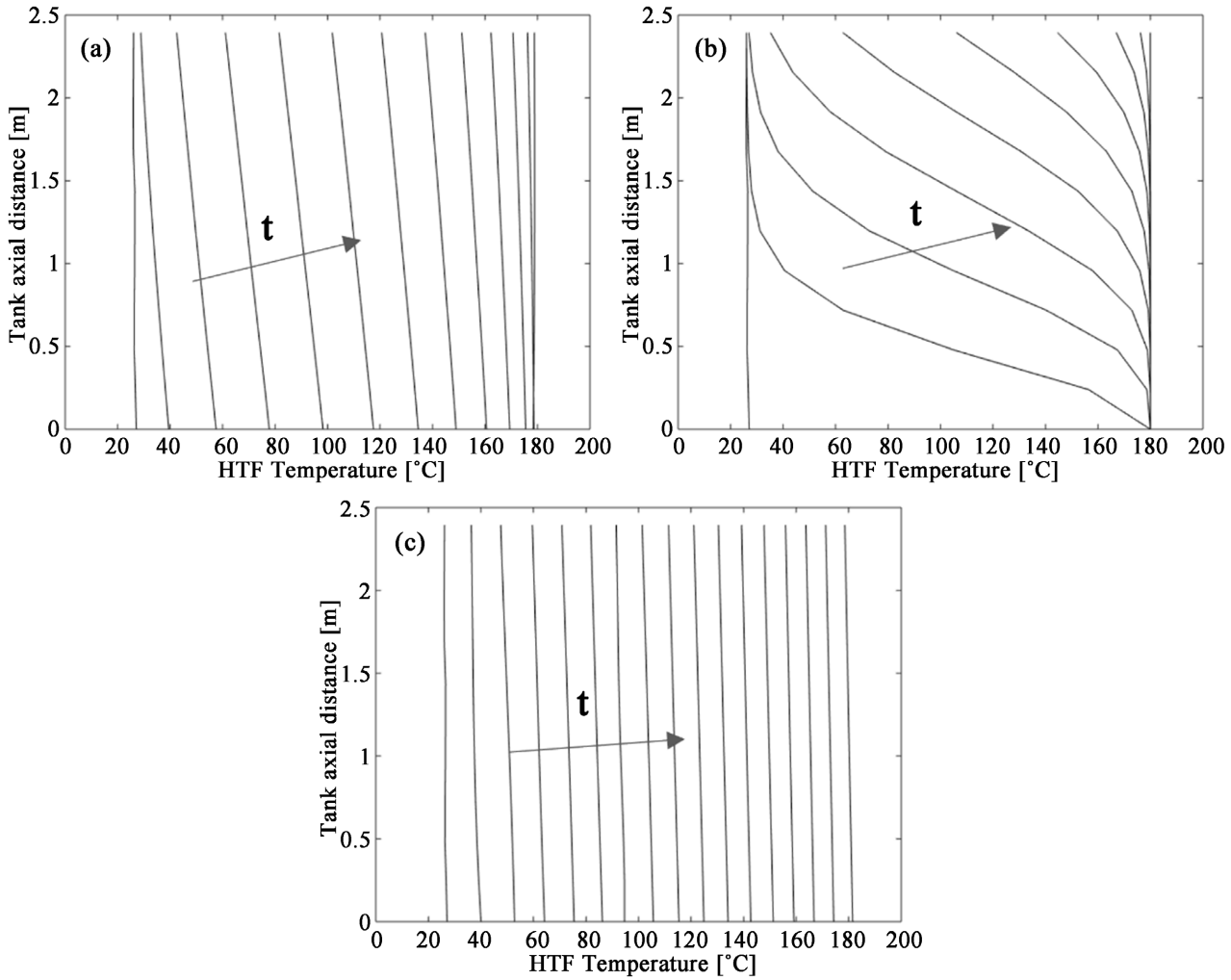

Figure 9. Axial temperature distribution for the three different inlet HTF profiles: increasing for a charging duration of 16 h and time interval of 1 h (a), constant for a charging duration of 1 h and time interval of 5 min (b) and solar collector field for a charging duration of 6 h and time interval of 30 min (c). (Axial distance measured from the top)

modes (depicted as a, b and c). As also indicated in Table 4, the charging process duration differs for each case following the respective inlet HTF condition. The reported charging duration and time interval are accordingly adjusted in Figure 9 to best illustrate the temperature profile of the tank during the charging process.

Figure 10 shows in a more illustrative manner how stratification develops in the tank for two of the three charging modes. More specifically, the stratification number is plotted vs a normalized time t/t_c, so that a common time range is used for all modes. It can be observed that for the constant inlet temperature case this number attains its highest value already from the start and this remains high for almost one third of the total charging cycle. It then reduces gradually and almost vanishes after two thirds of the cycle. In the case of input from a solar source, it is observed that the peak value of stratification is attained at about one third of the cycle and then the drop is almost linear until the end of the cycle. In the case

Table 4. Charging time and total stored energy per charging mode

	Charging time (h)	Stored energy (kWh)	Maximum $\overline{(\partial T/\partial z)_t}$ (˚C/m)
Increasing inlet HTF temperature	16	387.9	3.82
Constant inlet HTF temperature	1	329.5	64.27
Solar collector field inlet HTF temperature	6	340.0	7.06

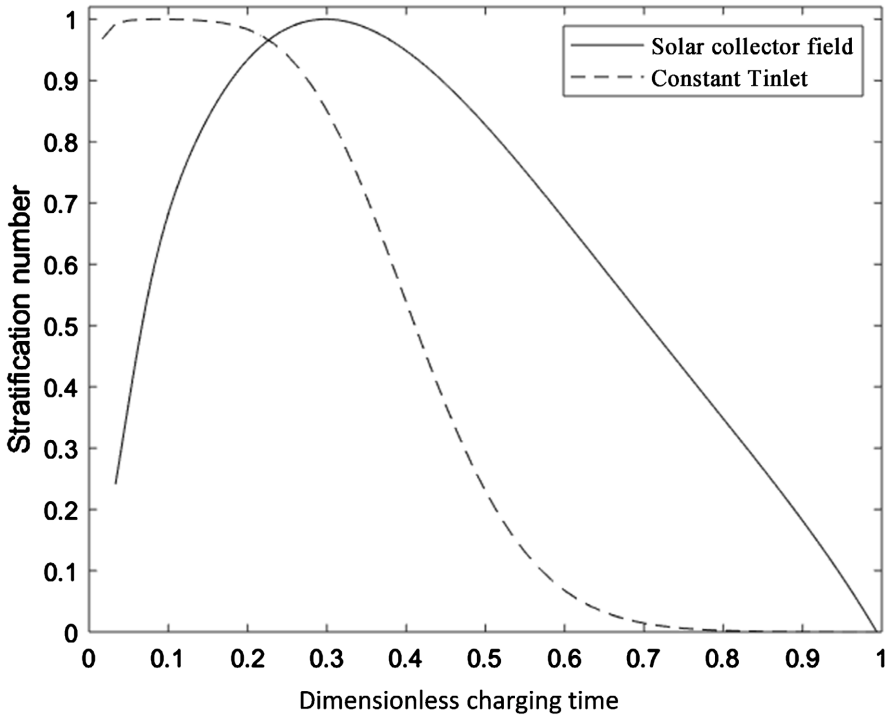

Figure 10. Stratification number for two different inlet HTF profiles during a charging cycle: constant inlet temperature and heating from solar collector field.

of increasing inlet temperature, the tank does not reach a uniform state, as the input HTF is constantly augmenting, but instead maintains a mild linear stratification at all times. As such, this case is omitted for this specific comparison.

Certainly, when the stratification numbers are considered in a non-normalized form they have quite different values, as can be seen in **Table 4**. In particular, the constant inlet HTF temperature mode presents the highest maximum value of Str, followed by the solar collector field charging and the increasing inlet HTF temperature.

The stratification number $Str(t)$ has been also used by Lugolole *et al.* [40], who used a variable inlet temperature in their oil-pebble storage tank experiments and the form of its time variation is similar to our results shown in **Figure 10** for the solar collector field inlet temperature, exhibiting peaks at the first half of the cycle, followed by a gradual decrease until the end of the cycle.

Additional results are presented in **Figure 11**, illustrating the inlet and outlet HTF temperature for the three charging modes. Charging modes 1 and 3 lead to

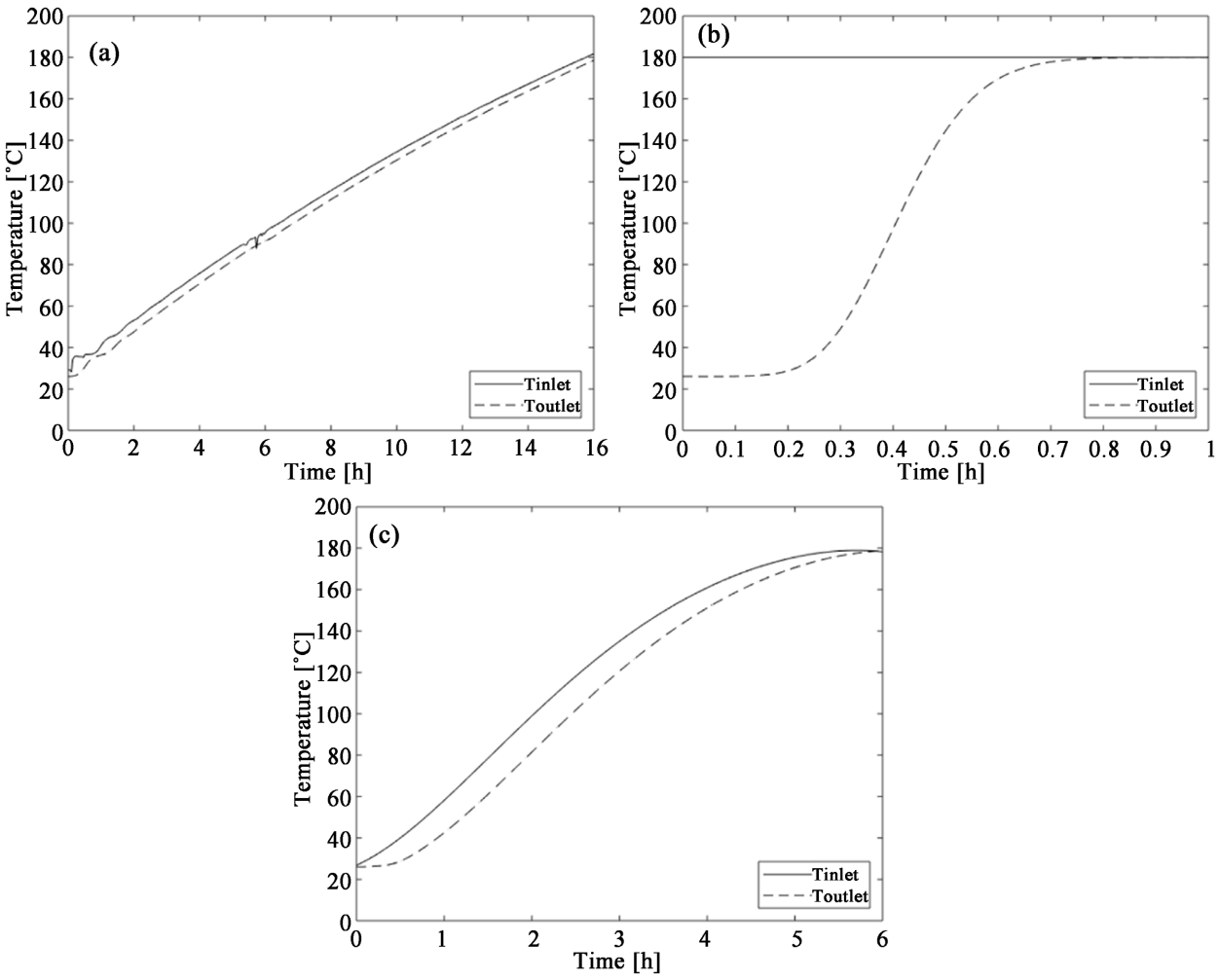

Figure 11. Inlet and outlet HTF temperature profiles for the three different inlet HTF profiles: increasing for a charging duration of 16 h and time interval of 1 h (a), constant for a charging duration of 1 h and time interval of 5 min (b) and solar collector field for a charging duration of 6 h and time interval of 30 min (c).

a nearly constant increase of the outlet HTF temperature, while mode 2 results in the formation of temperature difference between the top and the bottom parts of the tank. Minor fluctuations of the inlet HTF temperature values are noted, due to experimental uncertainties or possible instantaneous deficiencies of the equipment.

The total stored energy in the tank presents small differences between the examined scenarios, as previously discussed. Figure 12 presents the amount of stored energy with time. The first scenario presents a steady increase of the stored energy, the second one a steady increase until its full charging and the third one follows the solar collector energy yield (slower in the beginning and the end of the charging process).

Figure 13 presents the instantaneous charging efficiency for each of the scenarios. The inlet HTF temperature fluctuations of the first charging mode are propagated to this parameter as well (Figure 13(a)). The instantaneous charging efficiency in this case presents low values from the first hour and remains low

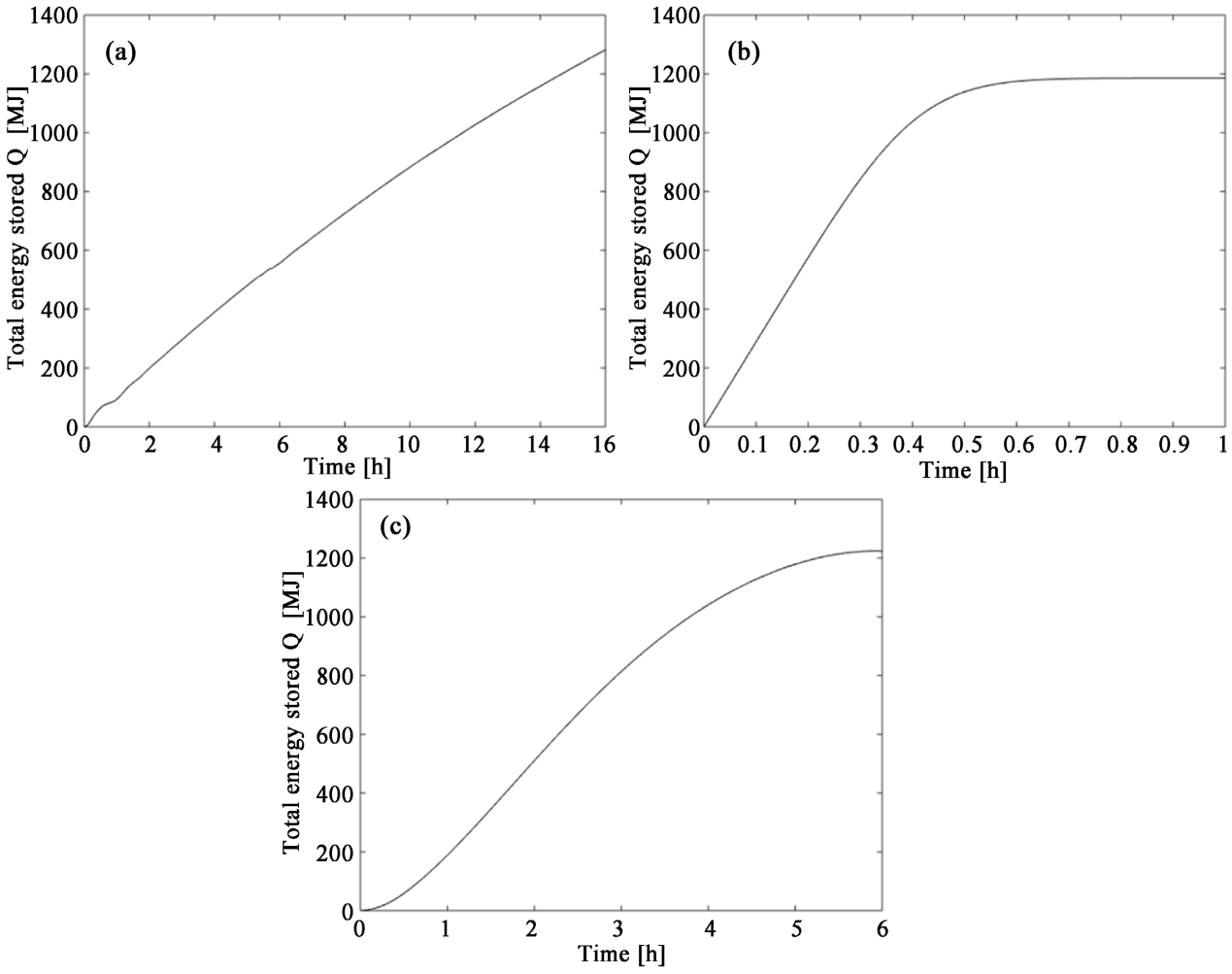

Figure 12. Total energy stored for the three different inlet HTF profiles: increasing for a charging duration of 16 h and time interval of 1 h (a), constant for a charging duration of 1 h and time interval of 5 min (b) and solar collector field for a charging duration of 6 h and time interval of 30 min (c).

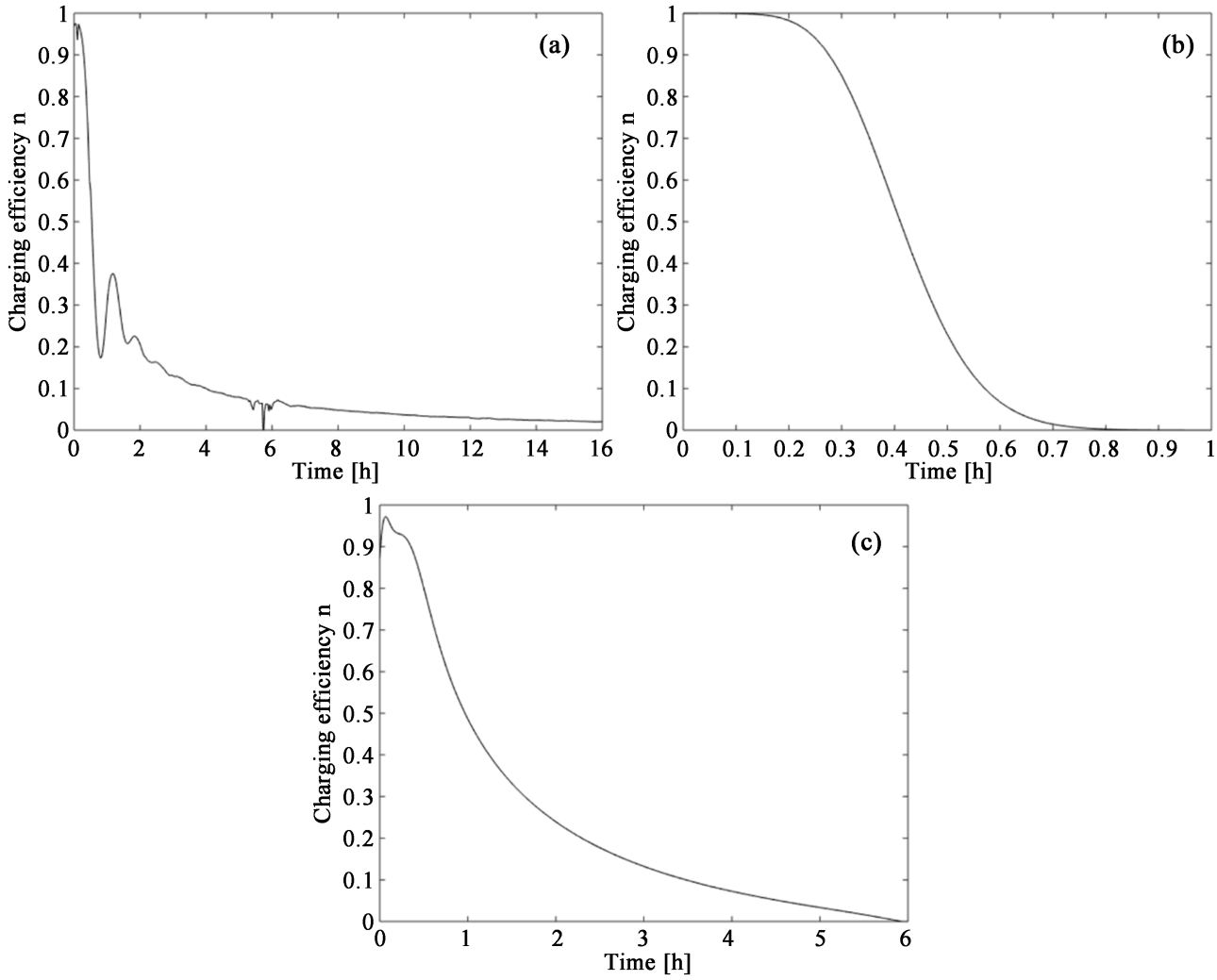

Figure 13. Instantaneous charging efficiency for the three different inlet HTF profiles: increasing for a charging duration of 16 h and time interval of 1 h (a), constant for a charging duration of 1 h and time interval of 5 min (b) and solar collector field for a charging duration of 6 h and time interval of 30 min (c).

throughout the charging process. The second mode results in higher energy efficiency values, in agreement with the continuously increased inlet HTF temperature and the fast charging time. Efficiencies above 0.5 are noted for almost half of the charging period in this case. Lastly, the third mode presents an intermediate performance compared to the two previous cases. Efficiencies above 0.5 are only observed for the first charging hour and are significantly lowered after that.

The general form of the efficiency curve in **Figure 13(c)** closely resembles the respective transient efficiency curves in the study of Mawire *et al.* [38], which is one of the few considering a variable inlet temperature. In fact, their time variation was similar to the one assumed for solar-field heating in the present work, and for almost the same duration of the charging process.

5. Conclusion

Packed bed TES applications have proved to be a promising addition to RES

systems for heat and power generation, improving efficiency, reliability and security. Nevertheless, numerical tools are required to better understand their performance and improve the design process. This study presents the method to develop a one-dimensional numerical model that solves the heat balance equations of a discretised tank and predicts the temperature evolution of the filler material and the heat transfer fluid across the axial direction of the tank. A magnetite ore based packed bed TES system is also presented and characterised under a thermal charging process. The model is validated through a solid approach, using data from two literature studies, as well as the experimental results of the presented packed bed tank. The model proves its accuracy under varying conditions, *i.e.*, different dimensions of the tank, filler material, heat transfer fluid, charging/discharging process and inlet temperature. Three charging modes of the tank are investigated based on varying and constant temperature profiles of the inlet HTF temperature, resulting in an analysis and comparison of obtained results. The model will be further developed to include thermal processes during a phase change, allowing the simulation of the performance of Phase Change Materials as a storage medium. The developed tools will be used in future studies to investigate an optimal TES tank configuration and operation in terms of FM, HTF, tank geometry and porosity, as well as charging conditions. The aim is also to conduct comparative studies between sensible and latent thermal storage applications, demonstrating the benefits and drawbacks of each case.

Acknowledgements

This research is co-financed by Greece and the European Union (European Social Fund—ESF) through the Operational Programme "Human Resources Development, Education and Lifelong Learning" in the context of the project "Reinforcement of Postdoctoral Researchers—2nd Cycle" (MIS-5033021), implemented by the State Scholarships Foundation (IKY).

Conflicts of Interest

The authors declare no conflicts of interest regarding the publication of this paper.

References

[1] Cabeza, L.F., Martorell, I., Miró, L., Fernández, A.I. and Barreneche, C. (2015) Introduction to Thermal Energy Storage (TES) Systems. In: Cabeza, L.F., Ed., *Advances in Thermal Energy Storage Systems*, Elsevier, Amsterdam, 1-28. https://doi.org/10.1533/9781782420965.1

[2] Cabeza, L.F. (2021) Advances in Thermal Energy Storage Systems. Elsevier, Amsterdam. https://doi.org/10.1016/B978-0-12-819885-8.00002-4

[3] White, A.J., McTigue, J.D. and Markides, C.N. (2016) Analysis and Optimisation of Packed-Bed Thermal Reservoirs for Electricity Storage Applications. *Proceedings of the Institution of Mechanical Engineers*, *Part A*: *Journal of Power and Energy*, **230**, 739-754. https://doi.org/10.1177/0957650916668447

[4] Ge, Y.Q., Zhao, Y. and Zhao, C.Y. (2021) Transient Simulation and Thermodynamic Analysis of Pumped Thermal Electricity Storage Based on Packed-Bed Latent Heat/Cold Stores. *Renew Energy*, **174**, 939-951. https://doi.org/10.1016/j.renene.2021.04.094

[5] Garg, H.P., Mullick, S.C. and Bhargava, A.K. (1985) Sensible Heat Storage. In: Garg, H.P., Mullick, S.C. and Bhargava, A.K., Eds., *Solar Thermal Energy Storage*, Springer, Dordrecht, 82-153. https://doi.org/10.1007/978-94-009-5301-7_2

[6] Stathopoulos, N. (2015) Numerical and Experimental Optimization of Peak Power Reduction Control Strategies. ENTPE, Lyon.

[7] Tamme, R., Bauer, T., Buschle, J., Laing, D., Müller-Steinhagen, H. and Steinmann, W.-D. (2008) Latent Heat Storage above 120˚C for Applications in the Industrial Process Heat Sector and Solar Power Generation. *International Journal of Energy Research*, **32**, 264-271. https://doi.org/10.1002/er.1346

[8] Kunwer, R., Pandey, S. and Pandey, G. (2022) Technical Challenges and Their Solutions for Integration of Sensible Thermal Energy Storage with Concentrated Solar Power Applications—A Review. *Process Integration and Optimization for Sustainability*, **6**, 559-585. https://doi.org/10.1007/s41660-022-00231-9

[9] Zhao, B., Cheng, M., Liu, C. and Dai, Z. (2017) An Efficient Tank Size Estimation Strategy for Packed-Bed Thermocline Thermal Energy Storage Systems for Concentrated Solar Power. *Solar Energy*, **153**, 104-114. https://doi.org/10.1016/j.solener.2017.05.057

[10] Mawire, A., Lentswe, K.A. and Shobo, A. (2019) Performance Comparison of Four Spherically Encapsulated Phase Change Materials for Medium Temperature Domestic Applications. *Journal of Energy Storage*, **23**, 469-479. https://doi.org/10.1016/j.est.2019.04.007

[11] Khor, J.O., Sze, J.Y., Li, Y. and Romagnoli, A. (2020) Overcharging of a Cascaded Packed Bed Thermal Energy Storage: Effects and Solutions. *Renewable and Sustainable Energy Reviews*, **117**, Article ID: 109421. https://doi.org/10.1016/j.rser.2019.109421

[12] Yang, X. and Cai, Z. (2019) An Analysis of a Packed Bed Thermal Energy Storage System Using Sensible Heat and Phase Change Materials. *International Journal of Heat and Mass Transfer*, **144**, Article ID: 118651. https://doi.org/10.1016/j.ijheatmasstransfer.2019.118651

[13] Ismail, K.A.R. and Stuginsky Jr., R. (1999) A Parametric Study on Possible Fixed Bed Models for Pcm and Sensible Heat Storage. *Applied Thermal Engineering*, **19**, 757-788. https://doi.org/10.1016/S1359-4311(98)00081-7

[14] Zaghari, R. and Baharloo-Houreh, N. (2022) A Comprehensive Review of Sensible Heat Based Packed Bed Solar Thermal Energy Storage System. *Journal of Renewable and New Energy*, **9**, 130-140.

[15] Fu, T., Zhu, G. and Tong, L. (2022) Numerical Investigation on Optimizing the Performance of Heat Transfer in Vertical Packed Bed at the Particle Scale. *Journal of Power and Energy Engineering*, **10**, 26-33. https://doi.org/10.4236/jpee.2022.1012003

[16] Mawire, A. and McPherson, M. (2009) Experimental and Simulated Temperature Distribution of an Oil-Pebble Bed Thermal Energy Storage System with a Variable Heat Source. *Applied Thermal Engineering*, **29**, 1086-1095. https://doi.org/10.1016/j.applthermaleng.2008.05.028

[17] Stathopoulos, N., El Mankibi, M., Issoglio, R., Michel, P. and Haghighat, F. (2016) Air-PCM Heat Exchanger for Peak Load Management: Experimental and Simula-

tion. *Solar Energy*, **132**, 453-466. https://doi.org/10.1016/j.solener.2016.03.030

[18] Stathopoulos, N., El Mankibi, M. and Santamouris, M. (2017) Numerical Calibration and Experimental Validation of a PCM-Air Heat Exchanger Model. *Applied Thermal Engineering*, **114**, 1064-1072. https://doi.org/10.1016/j.applthermaleng.2016.12.045

[19] Roccamena, L., El Mankibi, M. and Stathopoulos, N. (2019) Development and Validation of the Numerical Model of an Innovative PCM Based Thermal Storage System. *Journal of Energy Storage*, **24**, Article ID: 100740. https://doi.org/10.1016/j.est.2019.04.014

[20] Yagi, S. and Wakao, N. (1959) Heat and Mass Transfer from Wall to Fluid in Packed Beds. *AIChE Journal*, **5**, 79-85. https://doi.org/10.1002/aic.690050118

[21] Esence, T., Bruch, A., Molina, S., Stutz, B. and Fourmigué, J.F. (2017) A Review on Experience Feedback and Numerical Modeling of Packed-Bed Thermal Energy Storage Systems. *Solar Energy*, **153**, 628-654. https://doi.org/10.1016/j.solener.2017.03.032

[22] Ranz, W. and Marshall, W. (1952) Evaporation from Drops. *Chemical Engineering Progress*, **48**, 141-146.

[23] Li, P., Van Lew, J., Karaki, W., Chan, C., Stephens, J. and Wang, Q. (2011) Generalized Charts of Energy Storage Effectiveness for Thermocline Heat Storage Tank Design and Calibration. *Solar Energy*, **85**, 2130-2143. https://doi.org/10.1016/j.solener.2011.05.022

[24] Pacheco, J.E., Showalter, S.K. and Kolb, W.J. (2002) Development of a Molten-Salt Thermocline Thermal Storage System for Parabolic Trough Plants. *Journal of Solar Energy Engineering, Transactions of the ASME*, **124**, 153-159. https://doi.org/10.1115/1.1464123

[25] Hoffmann, J.F., Fasquelle, T., Goetz, V. and Py, X. (2016) A Thermocline Thermal Energy Storage System with Filler Materials for Concentrated Solar Power Plants: Experimental Data and Numerical Model Sensitivity to Different Experimental Tank Scales. *Applied Thermal Engineering*, **100**, 753-761. https://doi.org/10.1016/j.applthermaleng.2016.01.110

[26] Van Lew, J.T., Li, P., Chan, C.L., Karaki, W. and Stephens, J. (2011) Analysis of Heat Storage and Delivery of a Thermocline Tank Having Solid Filler Material. *Journal of Solar Energy Engineering*, **133**, Article ID: 021003. https://doi.org/10.1115/1.4003685

[27] Xu, C., Wang, Z., He, Y., Li, X. and Bai, F. (2012) Sensitivity Analysis of the Numerical Study on the Thermal Performance of a Packed-Bed Molten Salt Thermocline Thermal Storage System. *Applied Energy*, **92**, 65-75. https://doi.org/10.1016/j.apenergy.2011.11.002

[28] Hernandez, A.B., Uriz, I., Ortega-Fernández, I., Rodriguez-Aseguinolaza, J., Ortuondo, A. and Faik, A. (2018) Solid Packed Bed Thermal Energy Storage for ORC Electric Generation in Fresnel Type CSP Plants. *AIP Conference Proceedings*, **2033**, Article ID: 090013. https://doi.org/10.1063/1.5067107

[29] Technical Data Sheet Therminol® SP Heat Transfer Fluid. https://productcatalog.eastman.com/tds/ProdDatasheet.aspx?product=71093454

[30] Jacobs, R. and Bruno, F. (2021) Thermophysical Properties of Quartzite for High Temperature Thermal Storage.

[31] Grosu, Y., Faik, A., Ortega-Fernández, I. and D'Aguanno, B. (2017) Natural Magnetite for Thermal Energy Storage: Excellent Thermophysical Properties, Reversible Latent Heat Transition and Controlled Thermal Conductivity. *Solar Energy Mate-*

rials and Solar Cells, **161**, 170-176. https://doi.org/10.1016/j.solmat.2016.12.006

[32] Filali Baba, Y., Ajdad, H., Mers, A.A.L., Grosu, Y. and Faik, A. (2019) Multilevel Comparison between Magnetite and Quartzite as Thermocline Energy Storage Materials. *Applied Thermal Engineering*, **149**, 1142-1153. https://doi.org/10.1016/j.applthermaleng.2018.12.002

[33] Qiu, H., Wu, Y., Chen, H., Wang, R., Yu, J. and Lin, Y. (2023) Influence of SiC on the Thermal Energy Transfer and Storage Characteristics of Microwave-Absorbing Concrete Containing Magnetite and/or Carbonyl Iron Powder. *Construction and Building Materials*, **366**, Article ID: 130191. https://doi.org/10.1016/j.conbuildmat.2022.130191

[34] Pirtsul, A.E., Rubtsova, M.I., Mendgaziev, R.I., Cherednichenko, K.A., *et al.* (2022) Phase-Change Composites for Bimodal Solar/Electromagnetic Energy Storage Based on Magnetite-Modified Cellulose Microfibers. *Materials Letters*, **327**, Article ID: 132997. https://doi.org/10.1016/j.matlet.2022.132997

[35] Filali Baba, Y., Al Mers, A., Faik, A. and Ajdad, H. (2019) Experimental Characterization of Magnetite under Thermal Cycling for Thermocline Energy Storage. 13*th International Renewable Energy Storage Conference*, Dusseldorf, 12-15 March 2019, 81-85. https://doi.org/10.2991/ires-19.2019.10

[36] Ortega-Fernández, I., Hernández, A.B., Wang, Y. and Bielsa, D. (2021) Performance Assessment of an Oil-Based Packed Bed Thermal Energy Storage Unit in a Demonstration Concentrated Solar Power Plant. *Energy*, **217**, Article ID: 119378. https://doi.org/10.1016/j.energy.2020.119378

[37] Papanicolaou, E. and Belessiotis, V. (2009) Transient Development of Flow and Temperature Fields in an Underground Thermal Storage Tank under Various Charging Modes. *Solar Energy*, **83**, 1161-1176. https://doi.org/10.1016/j.solener.2009.01.017

[38] Mawire, A., McPherson, M., van den Heetkamp, R.R.J. and Mlatho, S.J.P. (2009) Simulated Performance of Storage Materials for Pebble Bed Thermal Energy Storage (TES) Systems. *Applied Energy*, **86**, 1246-1252. https://doi.org/10.1016/j.apenergy.2008.09.009

[39] Lou, W., Luo, L., Hua, Y., Fan, Y. and Du, Z. (2021) A Review on the Performance Indicators and Influencing Factors for the Thermocline Thermal Energy Storage Systems. *Energies* (*Basel*), **14**, Article No. 8384. https://doi.org/10.3390/en14248384

[40] Lugolole, R., Mawire, A., Lentswe, K.A., Okello, D. and Nyeinga, K. (2018) Thermal Performance Comparison of Three Sensible Heat Thermal Energy Storage Systems during Charging Cycles. *Sustainable Energy Technologies and Assessments*, **30**, 37-51. https://doi.org/10.1016/j.seta.2018.09.002

Abbreviations

DHW	Domestic hot water
CSP	Concentrated solar power
FM	Filler material
HTF	Heat transfer fluid
RES	Renewable energy sources
TES	Thermal energy storage

Nomenclature

Latin Letters

A	Area [m^2]
C_p	Specific heat capacity [$J \cdot kg^{-1} \cdot K^{-1}$]
ct	Charging time [s]
d	Diameter [m]
H	Height of tank [m]
h	Heat transfer coefficient [$J \cdot kg^{-1}$]
k	Conductivity [$W \cdot m^{-1} \cdot K^{-1}$]
Q	Energy [kWh]
Str	Stratification number
T	Temperature [˚C, K]
t	Physical time [s]
U	Natural convective heat transfer coefficient, tank level [$W \cdot m^{-2}$ K]
V	Volume [m^3]
Δt	Time interval [s]
Δy	Distance [m]
$\dot{m}$	Flow rate [$m^3 \cdot h^{-1}$]

Greek Letters

η	Charging efficiency
μ	Viscosity [$kg \cdot m^{-1} \cdot s^{-1}$]
ρ	Density [$kg \cdot m^3$]
φ	Tank porosity

Subscripts/Superscripts

a	Referring to heat transfer fluid
amb	Referring to ambient
i	Node position, axial direction
in	Referring to inlet
ini	Referring to initial
out	Referring to outlet
p	Referring to filler material
s	Referring to surface
sf	Referring to interstitial / superficial